

Head-Discharge Equations to Fit a Set of Physical Models of Dam Breach

Donald L. Baker ¹

Abstract

Head-discharge equations are fitted to a set of physical models of dam breach, covering 378 different geometries. The method of fitting consists of three aspects: 1) the integration of the ideal weir equation over the geometric boundaries of the notch, 2) use of the Buckingham Pi theorem to remove data with explainable deviations from the fitting, and 3) the use of simulated annealing to do the fitting, with an objective function of mean absolute relative error. The equations are applied to an additional 60 geometries to check scaling.

Author

¹ Ph.D. Soil Physics, 5001 West 5th Place, Stillwater, OK 74074-6703

Keywords

Dam breach, head-discharge, physical model, simulated annealing, Buckingham Pi

Scope of the paper

Before this analysis, the author had not studied in this field in nearly three decades. Therefore the scope of this work is limited to the application of simple weir flow concepts that are fitted to the data set by simulated annealing. Only the discharge coefficients are fitted. All other secondary effects, such as contraction, entrance velocity corrections and boundary layers are ignored, partly due as well to the limitations of the data set, for which only six head-discharge points were typically taken per geometry. While one may not be an expert in a field, it is nevertheless possible to consider basic equations and apply methods such as simulated annealing that work across many disciplines. The reference for simulated annealing cited here (Goffe, et al., 1994) comes from the Journal of Econometrics.

The physical model

Consider the case of water flowing in a trapezoidal notch through the trapezoidal embankment of a reservoir. The notch has a bottom width, b (units of length, L), at height, h_u (L), above the reservoir floor, with a sidewall angle of ϕ (rad) from the vertical, making a slope, m_s , horizontal to vertical (H:V). The embankment has an upstream angle of θ (rad) above the horizontal, making a slope, μ (H:V). The intersection of the notch with the upstream slope is called the crest of the resulting weir. In addition, the floor of the notch downstream of the crest can be dropped, h_h (L), below the crest, forming a rectangular channel below the crest, so that the water flowing into it can be an aerated waterfall, or nappe. Figure 1 shows one such condition with $h_h = h_u$. Vertical measurements are taken with respect to the elevation of the bottom width, b , with h_e positive upwards and h_h and h_u positive downwards.

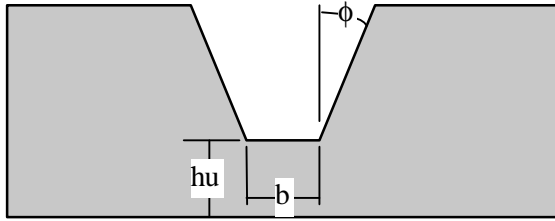


Figure 1a: View from Upstream

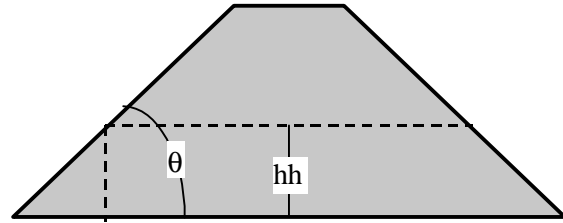


Figure 1b: Side View

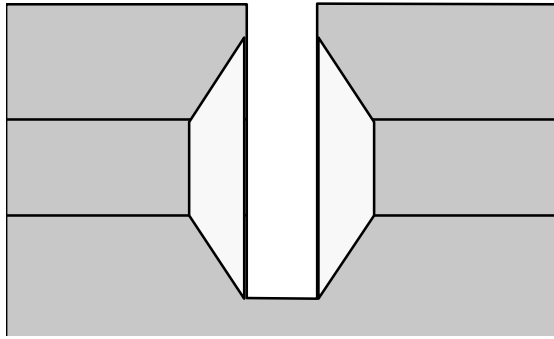


Figure 1c: Top View

This model was built and run at the Hydraulic Engineering Research Unit of the USDA Agricultural Research Service, Stillwater, OK. It was demonstrated in one geometry on June 27, 2001, to participants of the FEMA sponsored Workshop on Issues, Resolutions, and Research Needs Related to Dam Failure Analyses, Oklahoma City, OK. Three sets of data were generated. In the largest set the geometry combinations are: $b = 0.406\text{ m}$ (16 in); $h_u = 0\text{ m}$, 0.152 m (0.5 ft), 0.305 m (1 ft); $\mu = 0, 1, 2, 2.5, 3, 4, 6$; $h_h = 0\text{ m}$, 0.152 m (0.5 ft), 0.305 m (1 ft); and $m_s = 0, 0.25, 0.5, 1, 1.5, 2$. Two other sets were created to check scaling. For $b = 0.203\text{ m}$ (8 in), the variations are: $h_u = 0\text{ m}$, 0.152 m (0.5 ft), 0.305 m (1 ft); $\mu = 3$; $h_h = 0\text{ m}$, 0.152 m (0.5 ft), 0.305 m (1 ft); and $m_s = 0, 0.25, 0.5, 1, 1.5, 2$. For $b = 0.813\text{ m}$ (32 in), the variations are: $h_u = 0\text{ m}$, 0.305 m (1 ft); $\mu = 3$; $h_h = 0\text{ m}$, 0.152 m (0.5 ft), 0.305 m (1 ft); and $m_s = 0.5$.

Only two hydraulic measurements were made, the elevation, h_e (m), of the upstream reservoir above the crest of the notch, and the bulk flow of water, Q (m^3/s), through the notch.

Flow was measured with a differential manometer connected to orifice plates in a 0.3048 m (12 in) inlet pipe. The flow was typically set to six approximate levels of $Q = 0.00354, 0.00708, 0.01416, 0.02832, 0.05664, 0.08496, 0.1133, 0.1699, 0.2266$ or 0.3682 (m^3/s) (0.125, 0.25, 0.5, 1, 2, 3, 4, 6, 8 or 13 cfs), depending on the size of the notch. Then reservoir elevation was measured with point gage in a stilling well connected to a diffusing pipe on the bottom of the flume upstream of the Bernoulli drop at the notch.

Method of fitting

The method of fitting consists of three aspects: the integration of the ideal weir equation over the geometric boundaries of the notch, use of the Buckingham Pi theorem to remove data with explainable deviations from the fitting, and the use of simulated annealing to do the fitting.

According to basic texts (John and Haberman, 1988; Gupta, 1989) ideal flow, dQ (m^3/s), over an infinitesimal width, ds (m), of a weir (1) can be described by integrating the Bernoulli equation in the vertical, from the weir crest up to the level of the entrance head, h_e (m), under the assumptions that flow lines are parallel to the surface, the head is hydrostatic, the factors of friction, inertia and contraction are neglected, and the velocity of approach is neglected. Some measure of shear, inertia and contraction are brought back in with the empirically-determined discharge coefficient, C_d (dimensionless).

$$dQ = C_d \cdot \frac{2\sqrt{2g}}{3} \cdot h_e^{3/2} \cdot ds, \text{ where } g \text{ is the acceleration of gravity } (\text{m}/\text{s}^2) \quad (1)$$

If one integrates along the horizontal crest of the notch, $ds = 0$ to b , one gets a flow term related to $b \cdot h_e^{3/2}$. But if one integrates along an inclined line, $ds = 0$ to $\mu \cdot h_e$ or $m_s \cdot h_e$, one gets a flow term related to $h_e^{5/2}$. From a text such as Ackers, et al. (1978), one can see that

this applies to many channels or sharp or broad crested weirs with a trapezoidal flow cross section. One can show that if the integration is done at the level of the entrance head, h_e , along the inclined intersections of the upstream and side slopes and the horizontal crest in Figure 1, the result is equation (2), where a_0 and a_1 are dimensionless discharge coefficients.

$$Q_a = a_0 \cdot \frac{2\sqrt{2g}}{3} \cdot b \cdot h_e^{3/2} + a_1 \cdot \frac{8\sqrt{2g}}{15} \cdot (mu^2 + ms^2)^{1/2} h_e^{5/2} \quad (2)$$

But the data will show that if there is no drop (head cut) at the crest of the notch, $h_h = 0$, there is much less contribution from the upstream slope, mu . The resulting discharge relation looks more like (3).

$$Q_b = b_0 \cdot \frac{2\sqrt{2g}}{3} \cdot b \cdot h_e^{3/2} + b_1 \cdot \frac{8\sqrt{2g}}{15} \cdot ms \cdot h_e^{5/2} \quad (3)$$

This form is typical of a broad-crested weir or trapezoidal channel (Fread, 1991), while Q_a is more typical of the flow due to the drop of an free-falling, aerated jet (nappe) into a head cut channel, as we shall see.

Consider now a simpler form (4), where no assumption is made on the form of the second term. This form has four dimensioned variables, Q (m^3/s), h_e (m), b (m) and g ($9.80665 m/s^2$). According to the Buckingham Pi theorem (Logan, 1987), (4) can be rewritten in terms of two dimensionless π -variables, π_q and π_e , in (5).

$$Q = c_0 \cdot \frac{2\sqrt{2g}}{3} \cdot b \cdot h_e^{3/2} + c_1 \cdot \frac{8\sqrt{2g}}{15} \cdot h_e^{5/2} \quad (4)$$

$$\mathbf{p}_q = c_0 \cdot \frac{2\sqrt{2}}{3} + c_1 \cdot \frac{8\sqrt{2}}{15} \cdot \mathbf{p}_e = p_0 + p_1 \cdot \mathbf{p}_e, \quad \mathbf{p}_q = \frac{Q}{\sqrt{g \cdot b^2 \cdot h_e^3}}, \quad \mathbf{p}_e = \frac{h_e}{b} \quad (5)$$

Note that μ and m_s are already dimensionless π -variables, based on the ratios of lengths and heights of the upstream and channel side slopes. In addition, two more p-variables are defined: π_u (or π_{iu}) = h_u/b and π_h (or π_{ih}) = h_h/b for use in the fitting process. There is at least one more possible π -variable, the ratio of the full height of the embankment to b , but it is not necessary unless the flow overtops the embankment, which this data set did not address.

The linearity of (5) makes it easy to see when the data does not conform with the assumptions used in generating the equation. Then, either the data or the assumptions are bad. In Figure 2, for example, it is clear that the flow conforms to (5) for $h_h = 0$ m and for the lower values of π_e for $h_h = 0.15$ and 0.31 m. But for the higher values of h_e and $h_h = 0.15$ and 0.31 m, the value of π_q not only deviates from (5), it reaches a maximum and decreases, exhibiting non-monotonic behavior.

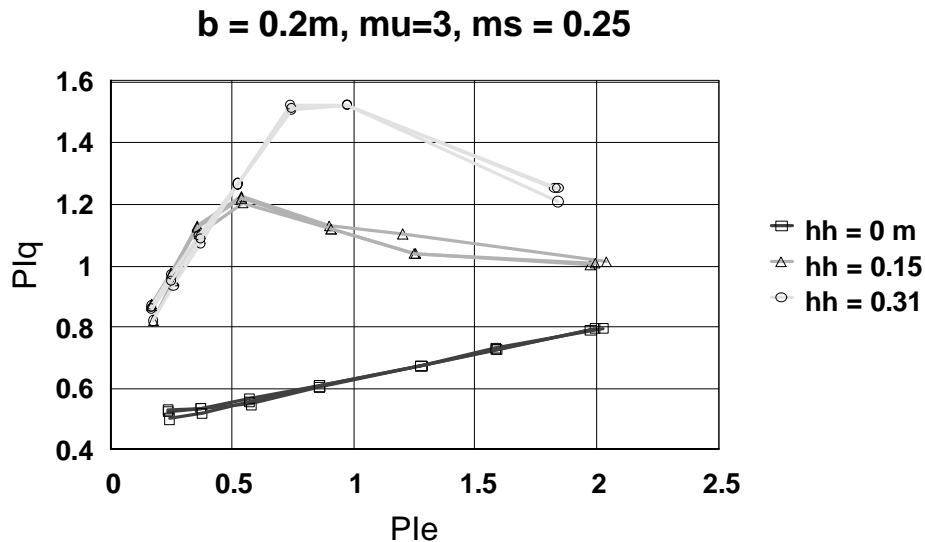


Figure 2: π_q versus π_e for $b = 0.2$ m, $h_u = 0, 0.15$ and 0.31 m, $\mu_u = 3$, $h_h = 0, 0.15$ and 0.31 m, and $m_s = 0.25$. Shows the decrease in flow when the jet is supported ($h_h = 0$ m), and when the jet presumably loses aeration.

This phenomenon presumably occurs when the jet loses aeration and becomes partially supported. One must say presumably because no data was taken to determine or verify at what values of $Q(\text{he})$ this might have happened. One might expect this drop; when the entrance head, h_e , becomes much larger than the modeled head cut drop, h_h , the flow should approach fully supported flow in the limit as h_e goes to infinity. As we can see from the bottom curve for $h_h = 0$, fully supported flow is much less than aerated flow. Since the decreasing flows for $h_h = 0.15$ and 0.31 are gross deviations from (5), one can legitimately remove this data from the fitting and set it aside for fitting to a separate or modified equation. This exclusion has been done manually with the largest data set for $b = 0.406$ m.

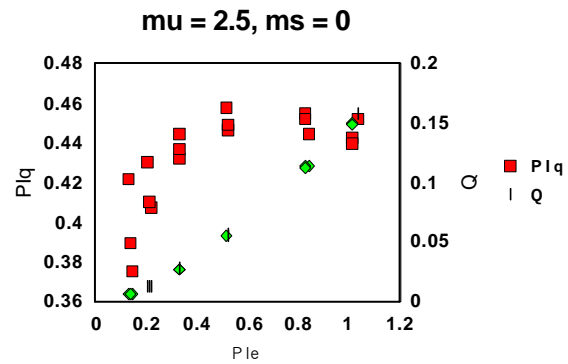
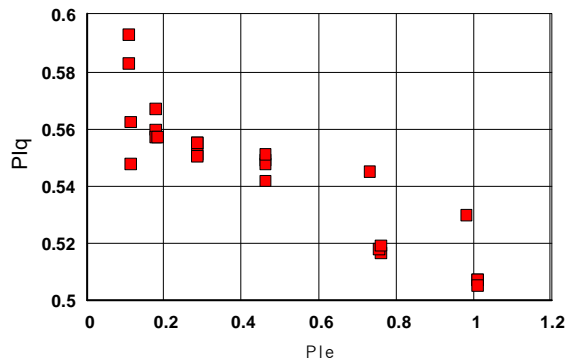


Figure 3a: Aerated jet πq vs π_e , for $b = 0.41$ m, $h_u = 0, 0.15$ and 0.31 m, $\mu = 0$, $h_h = 0.15$ m, and $m_s = 0$. Shows negative slope and an apparent scatter in some points below $\pi_e = 0.2$.

Figure 3b: Supported jet, πq and q vs π_e , for $b = 0.41$ m, $h_u = 0, 0.15$ and 0.31 m, $\mu = 2.5$, $h_h = 0$, and $m_s = 0$. Shows how the data does not conform to (5) for $m_s = 0$ and $h_h = 0$.

Figures 3a and 3b show other types of non-conformities to equation (5). In 3a, there is some scatter in the points for $\pi_e < 0.2$ and $\pi_e > 0.7$ for which the author has no explanation. Some of the points like this in the $b = 0.406$ m data set were removed before fitting, but it is also surprising to find the slope of the $\pi q(\pi_e)$ relation to be negative. In 3b, the points seem to have little, if any, relation to (5), even though the $Q(h_e)$ relation is monotonically increasing. The true relation seems to depend on powers of h_e other than $3/2$ or $5/2$. Most of the data for

supported jets with $ms = 0$ seemed to fall into this category. These points were left in the fitting process for the lack of a suitable alternative explanation for how they should be fitted.

To improve the possible fits for flow with an aerated jet, the data for $b = 0.406$ m and $hh = 0.15$ m and 0.31 m were lumped together after removing the values with obvious deviations due to the presumed lack of aeration. The remaining data for $b = 0.406$ m and $hh = 0$ m was designated as due to a fully supported jet and fitted separately.

The simulated annealing program, `simann.f` or `simann.for` (Goffe, et al., 1994), commonly available through NetLib, was adapted for this work. It has been found at:

<http://www.ukc.mirror.ac.uk/sites/netlib.bell-labs.com/netlib/opt/>

<http://ww.netlib.no/netlib/opt/index.html> and

<http://scicomp.ewha.ac.kr/netlib/opt/>

Simulated annealing can take much longer to run than methods of steepest descent because of its dependence on random guesses. But it can be more robust because it can step out of local minima to find the global minimum. Since it does not require an objective function that is quadratic, others can be used that allow better fitting over orders of magnitude of values, such as the mean absolute relative error (6), which is a form of percent error. If any of the predicted Q_i were less than or equal to zero, a severe penalty was added to f_{opt} in the program.

$$f_{opt} = \frac{1}{n} \sum_{i=1}^n \left| \frac{\hat{Q}_i - Q_i}{\sqrt{\hat{Q}_i \cdot Q_i}} \right| = \frac{1}{n} \sum_{i=1}^n rel_i \quad (6)$$

First, equation (5) was fitted to the aerated and supported jet data sets for $b = 0.406$ m for each of 126 separate geometries, (π_u, μ, m_s) , with the π_{ih} variations separated or lumped together as stated before. Then c_0 and c_1 were plotted against pairs of (π_u, μ, m_s) with TableCurve 3-D (tm SPSS, Inc.) to determine the most likely functions of a_0, a_1, b_0 and b_1 with (π_u, μ, m_s) . Then prototype relations of (3), (4) or (5) were fitted to all of the modified data ($b = 0.406$ m) for aerated jets and separately for supported jets. The function chosen to represent aerated jets was then compared to the $b = 0.203$ and $b = 0.813$ data to see if it scaled properly. The same was done for the function chosen to represent supported jets. The issue of partially supported jets was left for later analysis.

It is possible to fit (5) with a chi-square method (Press, et al., 1989), and the initial results will be much the same. But this approach has to be abandoned when the discharge coefficients become nonlinear functions of (π_u, μ, m_s) .

Results for aerated jet data

Equation (5) was fitted separately to each of the 126 different geometries of (μ, m_s, π_u) in the aerated jet data set, which excluded (π_e, π_q) points with obvious drops due to the supposed partial support of the jet by lack of aeration. Figure 4a shows the distribution of the (c_0, c_1) coefficients, with a limit of $0 \leq c_1 \leq 6$. Figure 4b shows the same distribution with the value of the relative error objective function, $rel(6)$, in the z-axis.

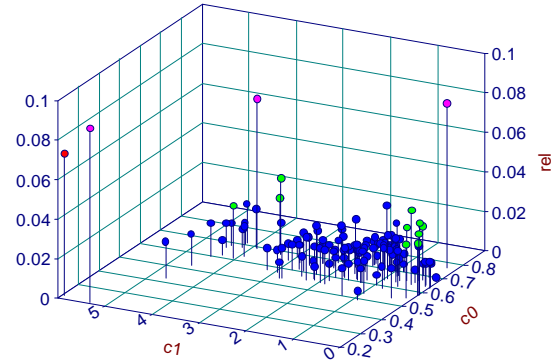
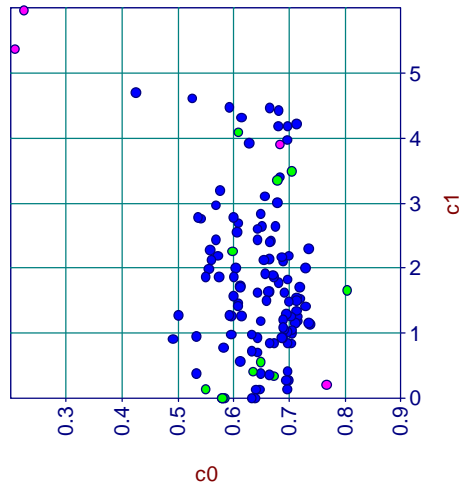


Figure 4a: c1 versus c0 for aerated jet data

Figure 4b: Relative absolute error, rel(c0,c1)

Figures 5a through 5f show plots of second-order fits of $(\mu, ms, \pi u)$ to $c0$ and $c1$. In the case of πu , it is apparent that the effect on $c0$ and $c1$ is the same for $\pi u = 0.375$ and 0.75 , but different for $\pi u = 0$. This might be caused by a transition close to $\pi u = 0$ that occurs over values of πu much smaller than 0.375 . It is simulated here with the use of the exponential function, $e^{-30\pi u}$, but it is not necessary to use an exponential function to achieve the same effect. Nor is it justified when the actual transition function is unknown.

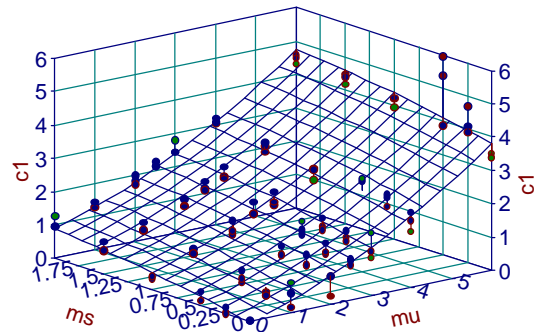
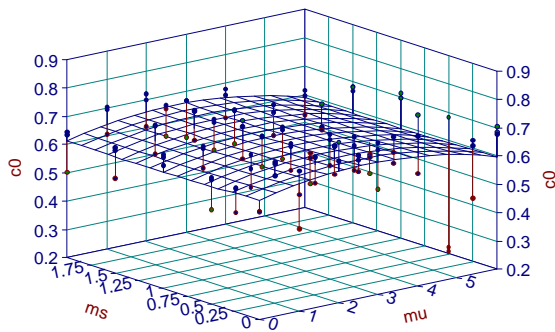


Figure 5a: $c0 \cong a+b\cdot\mu+c\cdot\mu^2+d\cdot ms+e\cdot ms^2$, $r^2 = 0.092$

Figure 5b: $c1 \cong a+b\cdot\mu+c\cdot\mu^2+d\cdot ms+e\cdot ms^2$, $r^2 = 0.948$

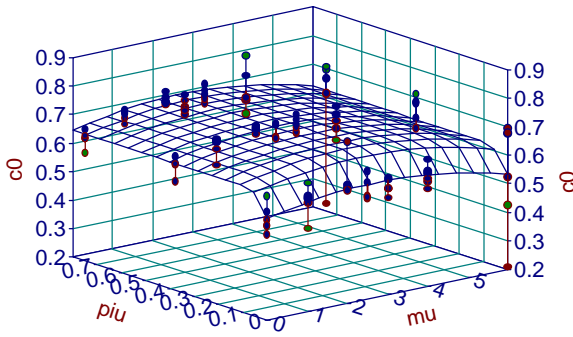


Figure 5c: $c_0 \cong a+b \cdot \mu+c \cdot \mu^2+d \cdot \exp(-30 \cdot \pi_u)$,
 $r^2 = 0.366$

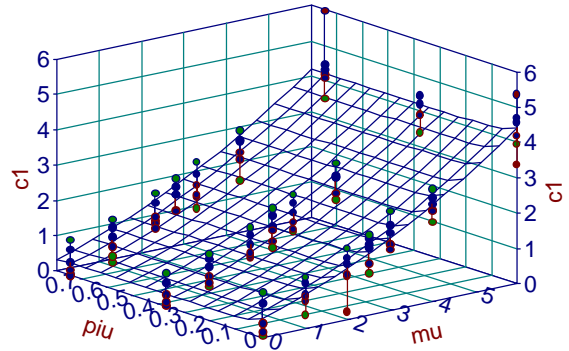


Figure 5d: $c_1 \cong a+b \cdot \mu+c \cdot \mu^2+d \cdot \exp(-30 \cdot \pi_u)$,
 $r^2 = 0.884$

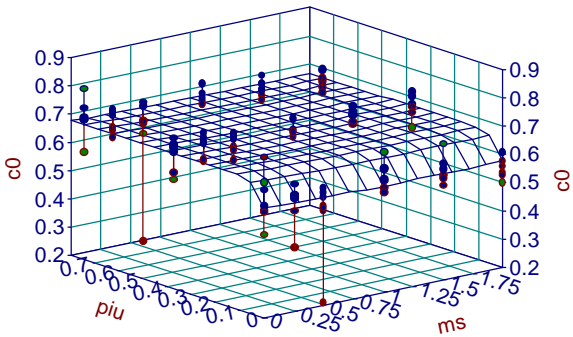


Figure 5e: $c_0 \cong a+b \cdot m_s+c \cdot m_s^2+d \cdot \exp(-30 \cdot \pi_u)$,
 $r^2 = 0.279$

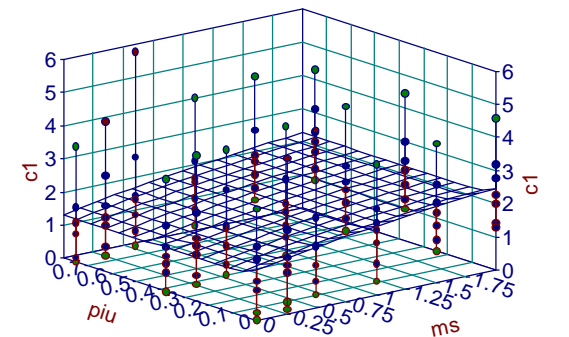


Figure 5f: $c_1 \cong a+b \cdot m_s+c \cdot m_s^2+d \cdot \exp(-30 \cdot \pi_u)$,
 $r^2 = 0.075$

It may be justified to use higher orders than second in fitting functions of μ and m_s to c_0 and c_1 . But there is little visual evidence of strong higher order effects in these plots, and the r^2 values for higher order fits provided by TableCurve 3-D did not improve greatly. Nor is there much evidence that the $(\mu^2 + m_s^2)^{1/2}$ term in (2) is entirely necessary. The fit of $c_1 = a \cdot \mu^b + c \cdot m_s^d$ is very similar to Figure 5b and has virtually the same value of r^2 .

Four different variations of (5) were fitted to the aerated jet data set. In each case, the (π_e, π_q) data points for all the 126 geometries were lumped together, and the coefficients of the

equation were varied by simulated annealing until the objective function, fobj (6), was sufficiently minimized. Some of the significant program parameters were: T(initial temperature) = 100, max = .false., eps = 10^{-7} , ns = 20, nt = 5, maxevl = 400000, c(i) = 2, vm(i) = ub(i) – lb(i).

All four used the same first term (7) with variations on the second term (8a-d), where the definition of ub is the same for all:

$$\frac{2\sqrt{2}}{3} \left(a_0 + a_1 \cdot \mu + a_2 \cdot \mu^2 + a_3 \cdot ms + a_4 \cdot ms^2 + ua \right) \quad (7)$$

$$ua = \begin{cases} a_5, & \mathbf{p}u = 0 \\ 0, & \mathbf{p}u > 0 \end{cases}$$

$$\frac{8\sqrt{2}}{15} \left(b_0 + b_1 \cdot \mu + b_2 \cdot \mu^2 + b_3 \cdot ms + b_4 \cdot ms^2 + ub \right) \cdot \mathbf{p}e \quad (8a)$$

$$ub = \begin{cases} b_5, & \mathbf{p}u = 0 \\ 0, & \mathbf{p}u > 0 \end{cases}$$

$$\frac{8\sqrt{2}}{15} (b_0 + ub) \cdot \left(b_1 \cdot \mu + b_2 \cdot \mu^2 + b_3 \cdot ms + b_4 \cdot ms^2 \right) \cdot \mathbf{p}e \quad (8b)$$

$$\frac{8\sqrt{2}}{15} \left(b_0 + b_1 \cdot \mu^{b_2} + b_3 \cdot ms^{b_4} + ub \right) \cdot \mathbf{p}e \quad (8c)$$

$$\frac{8\sqrt{2}}{15} (b_0 + ub) \cdot \left(b_1 \cdot \mu^{b_2} + b_3 \cdot ms^{b_4} \right) \cdot \mathbf{p}e \quad (8d)$$

Let the ratio inside the summation of (6) be called the relative error, rel, but for πq instead of Q. The result is the same because the common factor of $1/(g \cdot b^2 \cdot h e^3)^{1/2}$ cancels out. Table 1 shows the results of each equation set where rel is calculated for each individual point set (πe , πq), and the mean and standard deviation of rel are taken. The means of rel for the equation

sets using (8a) and (8c) are the same at the 3.4% significance level. The probability that the means for the sets using (8a) and (8b) are different is 79.3%. So it does not improve the results to use the term $(a \cdot \mu^b + c \cdot ms^d)$ over the quadratic terms in (8a) and (8c). But it does make a small amount of difference to calculate $(b_0 + ub)$ as a separate factor in the second term.

Table 1: Mean and standard deviation of the relative absolute error of each fitted πq point for aerated jet data, by equation set, $\pi q^{\wedge} = (7) + (8x) \cdot \pi e$.				
Equation	(7) + (8a)	(7) + (8b)	(7) + (8c)	(7) + (8d)
Mean rel	0.029743	0.032811	0.030124	0.033135
Std dev rel	0.034141	0.036120	0.034578	0.037318

Suppose that we are uncomfortable with the idea that there should be a contribution from the second $(he^{5/2})$ term when both $\mu = 0$ and $ms = 0$. Since there is no advantage to using powers of μ and ms , let us use the fit of (7) + (8b). Note that b_0 is not strictly independent of the values of b_1 through b_4 ; it is possible to get other values than those given here, so long as the value of $b_0 \cdot b_1$ is relatively constant. This analysis produced: $a_0 = 0.63092$, $a_1 = 0.03208$, $a_2 = -0.004415$, $a_3 = 0.03107$, $a_4 = -0.022192$, $a_5 = -0.057641$, $b_0 = 0.37219$, $b_1 = 0.98955$, $b_2 = 0.09486$, $b_3 = 0.93262$, $b_4 = 0.26304$, and $b_5 = 0.013031$.

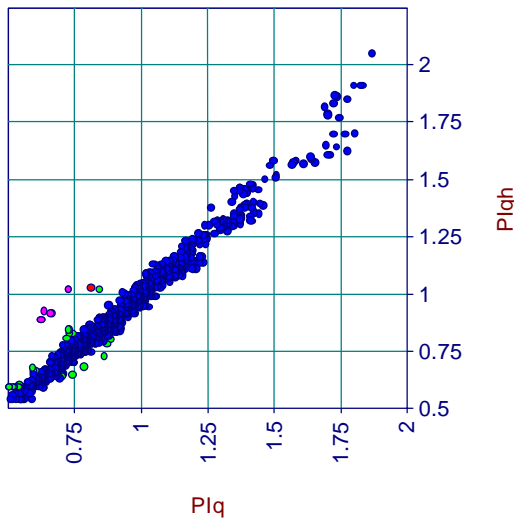


Figure 6a: Fitted πq^{\wedge} ($PIqh$) versus measured πq (PIq) for aerated jet data with $b = 0.406$ m

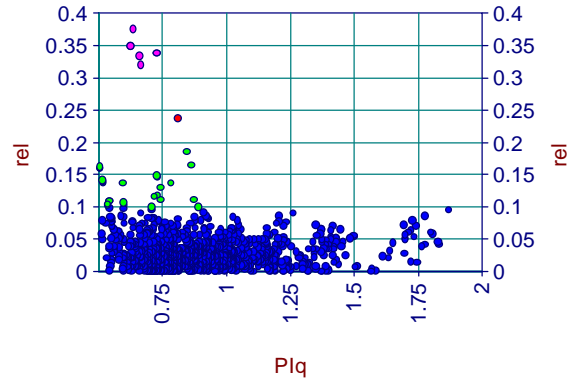


Figure 6b: Relative error, rel , in fitted πq^{\wedge} versus measured πq for aerated jet data with $b = 0.406$ m

Figures 6a and 6b illustrate the goodness of the fit for the aerated jet data with $b = 0.406$ m (16 in) for equations (7) + (8b). When rel (6) is calculated for each point separately, mean $rel = 0.0328$ with a standard deviation of 0.0361. For this experiment, the percentage error in reading the manometers attached to the orifice plate was estimated to be about 1.3% overall.

Figures 7a to 7b show the fit of the equation (7) + (8b) to measured data for $b = 0.406$ m (8 in). Here, the measured data has been divided into aerated jet data and presumably non-aerated or partially supported jet data by the obvious deviations from equation (5). When the data from both types is lumped together we get mean $rel = 0.2362$ with a standard deviation of 0.3192. When the measured data that obviously does not fit equation (5) is excluded, mean $rel = 0.0637$ with a standard deviation of 0.0786.

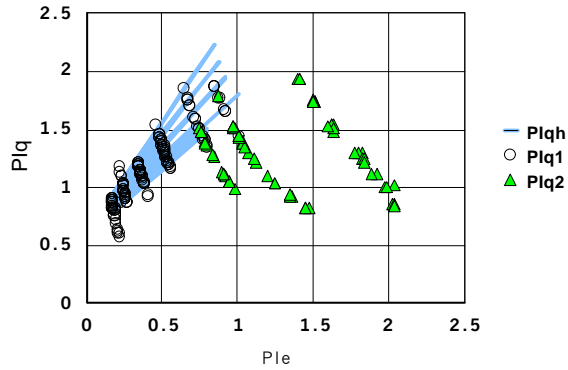


Figure 7a: Scaling plot for $b = 0.203$ (8 in) data, with fitted data, $PIqh$ (lines), measured aerated jet data, $PIq1$ (circles) and measured partially supported jet data, $PIq2$ (triangles) versus dimensionless head, PIe .

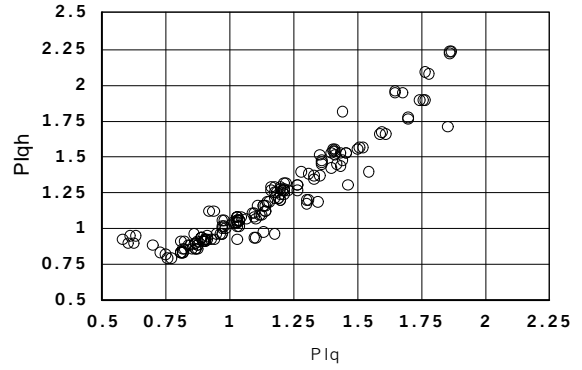


Figure 7b: Scaling plot for $b = 0.203$ m (8 in) data, with fitted data, $PIqh$ (circles) versus measured aerated jet data, PIq .

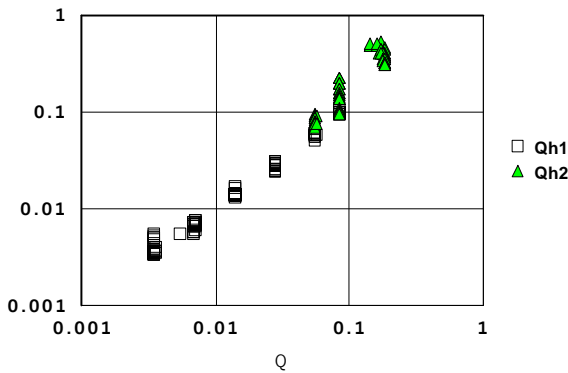


Figure 7c: Scaling plot for $b = 0.203$ m, with fitted aerated jet data, $Qh1$, and fitted partially supported jet data, $Qh2$, versus measured data, Q

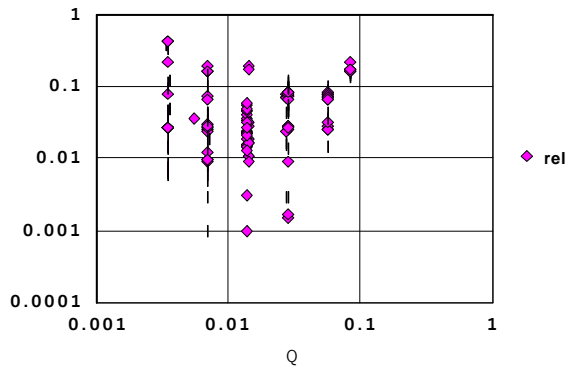


Figure 7d: Scaling plot for $b = 0.203$ m, with relative error, rel , versus measured data, Q (m^3/s)

Figures 8a through 8c show similar data for $b = 0.813$ m (32 in). The largest errors occur for $hh = 0.152$ m (0.5 ft), or $\pi u = 0.1875$, and for $\pi q < 0.65$. If all the data is considered, the fit produces a mean relative error, $rel = 0.0671$ with a standard deviation of 0.0690. If the data that obviously involves the presumed support of the jet is excluded, mean $rel = 0.0489$ with a

standard deviation of 0.0481. The author has no explanation for the apparent drop in the measured flow for low values compared to the estimated flow.

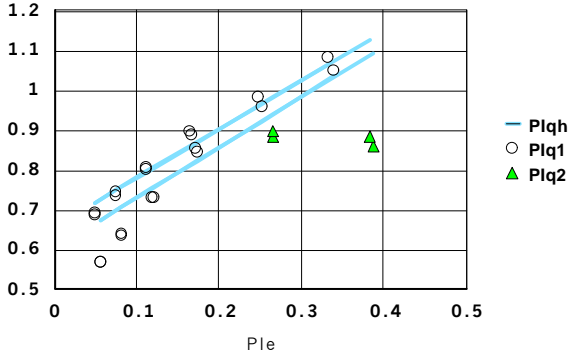


Figure 8a: Scaling plot for $b = 0.813$ m (32 in) data, with fitted data, PI_{qh} (lines), measured aerated jet data, PI_{q1} (circles) and measured partially supported jet data, PI_{q2} (triangles) versus dimensionless head, PI_e .

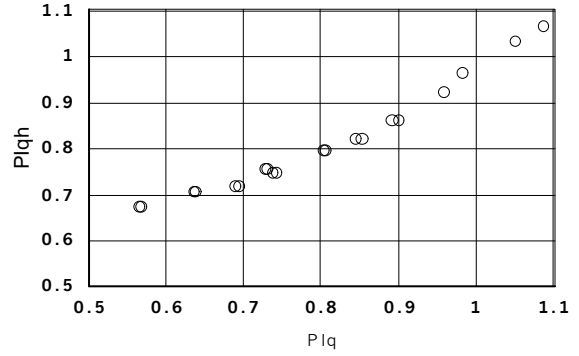


Figure 8b: Scaling plot for $b = 0.406$ m data, with fitted data, PI_{qh} (circles) versus measured aerated jet data, PI_q .

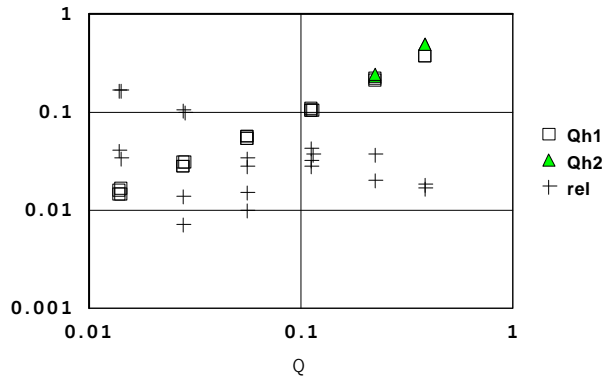


Figure 8c: Scaling plot for $b = 0.813$ m, with fitted aerated jet data, Q_{h1} , fitted partially supported jet data, Q_{h2} , and relative error, rel , versus measured data, Q (m^3/s).

Results for supported jet data

For the supported jet data, we have no obvious excuses to exclude any data for separate analysis. All of the data for $b = 0.406$ m (16 in) and $hh = 0$ ($\pi h = 0$) was fitted to equation (5) separately for each of the 126 (μ , ms , πu) geometries. Figure 9 shows the fitting results of c_0 , c_1 and rel . The layered effect in 9a comes from a strong relation of $ms + a = b \cdot c_0 + d \cdot c_1$, with $r^2 = 0.991$, where ms has six distinct values in this set of geometries.

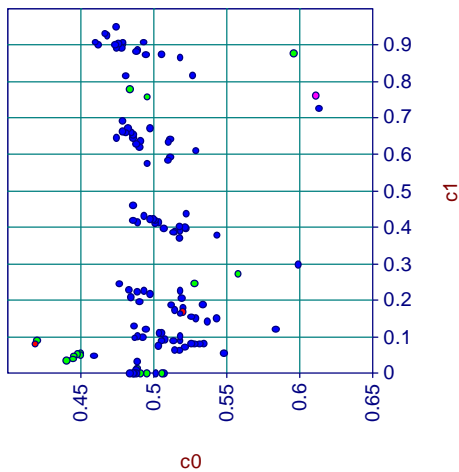


Figure 9a: c_1 versus c_0 for supported jet data

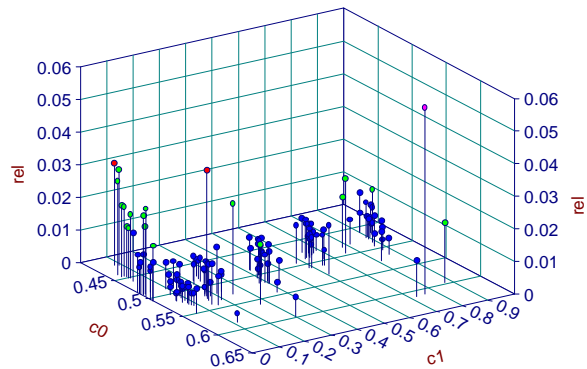


Figure 9b: $rel(c_0, c_1)$ for supported jet data

For this data, the effects of μ was much less significant and the effects of ms became significant in the third power. The effects of πu became neglectable. Figures 10a to 10e show how quadratic and cubic equations in ms produce the main effect on c_0 and c_1 in (5).

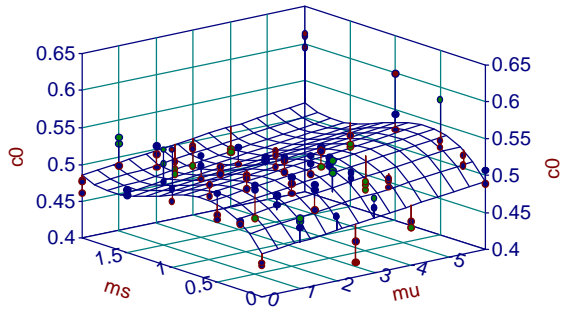


Figure 10a: $c_0 \cong a+b\cdot\mu+c\cdot ms+d\cdot ms^2+e\cdot ms^3$, $r^2 = 0.346$, supported jet data for $b = 0.406$ m

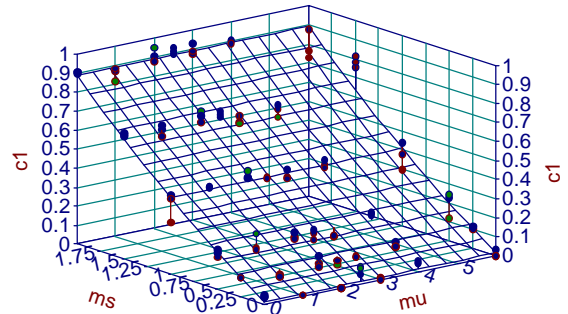


Figure 10b: $c_1 \cong a+b\cdot\mu+c\cdot ms+d\cdot ms^2$, $r^2 = 0.980$, supported jet data for $b = 0.406$ m

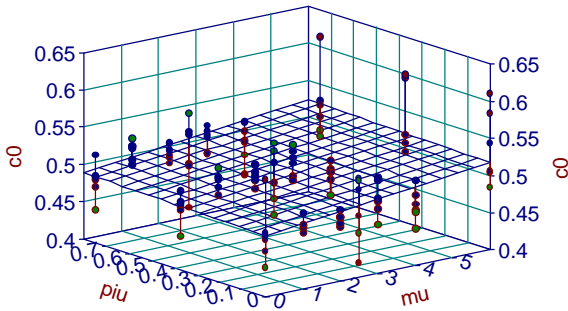


Figure 10c: $c_0 \cong a+b\cdot\mu+c\cdot\pi_u$, $r^2 = 0.117$, supported jet data for $b = 0.406$ m

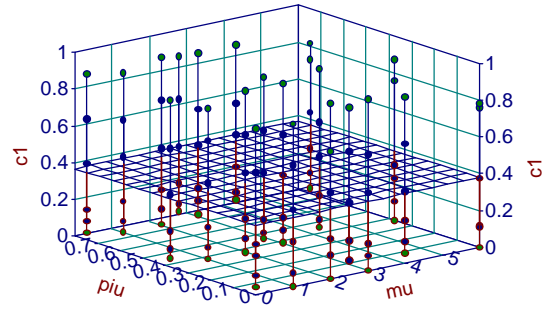


Figure 10d: $c_1 \cong a+b\cdot\mu+c\cdot\pi_u$, $r^2 = 0.0001$, supported jet data for $b = 0.406$ m

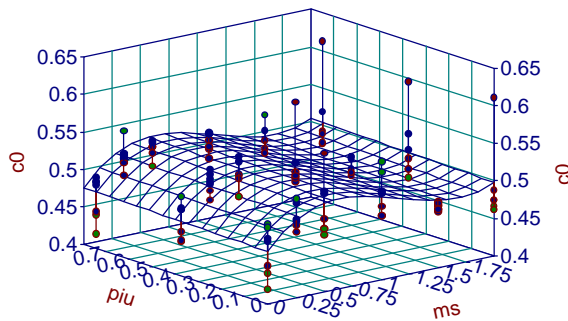


Figure 10e: $c_0 \cong a+b\cdot ms+c\cdot ms^2+d\cdot ms^3+e\cdot\pi_u$, $r^2 = 0.242$, supported jet data for $b = 0.406$ m

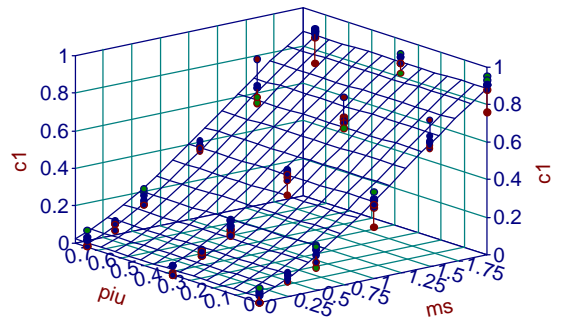


Figure 10f: $c_1 \cong a+b\cdot ms+c\cdot ms^2+d\cdot ms^3+e\cdot\pi_u$, $r^2 = 0.982$, supported jet data for $b = 0.406$ m

Several equations were fitted to the entire data set for fully supported jets with $b = 0.406$ m. For the higher order coefficients, including u_a and u_b as in (7) and (8), the mean relative absolute error was about 0.0215 or 0.0216, with a standard deviation of about 0.027. Equation (9) produced $\text{mean rel} = 0.02391$ with a standard deviation of 0.02823.

$$\begin{aligned}
 \mathbf{p}q = & \frac{2\sqrt{2}}{3} \left(a_0 + a_1 \cdot \mu u + a_2 \cdot ms + a_3 \cdot ms^2 + a_4 \cdot ms^3 \right) \\
 & + \frac{8\sqrt{2}}{15} \left(b_1 \cdot \mu u + b_2 \cdot ms + b_3 \cdot ms^2 \right) \cdot \mathbf{p}e
 \end{aligned} \tag{9}$$

In this equation, most of the coefficients with values on the order of 10^{-3} were dropped, which could have included a_1 and b_1 . Those remaining are $a_0 = 0.47099$, $a_1 = 0.002915$, $a_2 = 0.10965$, $a_3 = -0.11202$, $a_4 = 0.029651$, $b_1 = 0.001102$, $b_2 = 0.37215$ and $b_3 = 0.036534$. Figures 6a and 6b show the goodness of the fit of $\hat{\pi}q$ from the equation versus measured πq . The leftward tail at the bottom left of Figure 11a seems to indicate a drop in flow, πq , compared to the estimated flow, $\hat{\pi}q$, for which the author has no explanation.

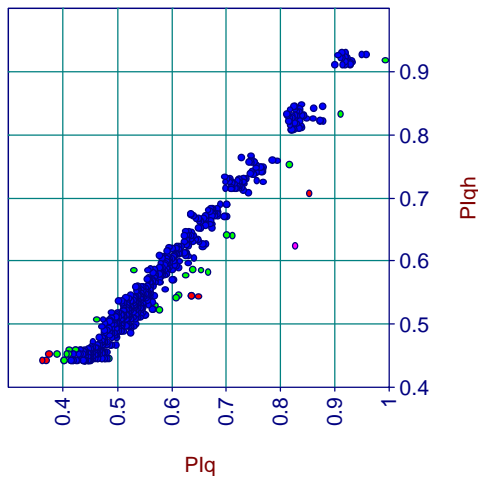


Figure 11a: Fitted $\hat{\pi}q$ ($PIqh$) versus measured πq (PIq) for supported jet data, $b = 0.406$ m

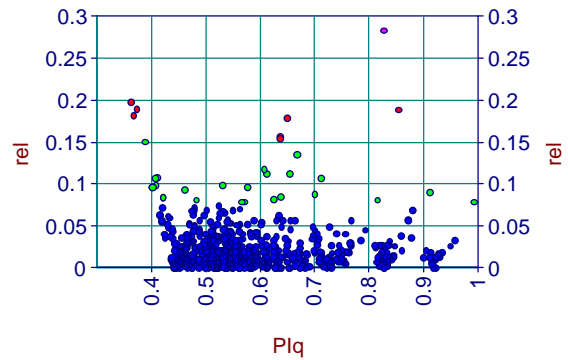


Figure 11b: Relative error, rel in fitted $\hat{\pi}q$ versus measured πq for supported jet data, $b = 0.406$ m

Figures 12a to 12d show the scaling of equation (9) estimates at $b = 0.203$ m (8 in). The mean of the relative absolute error, rel , for each data point is 0.0659 with a standard deviation of 0.1152. If the points with $rel > 0.1$ are discarded, then the mean rel drops to 0.0319 with a standard deviation of 0.0245. But in this case, there is no apparent justification for throwing those points away based on a supposed ability to fit them with another equation.

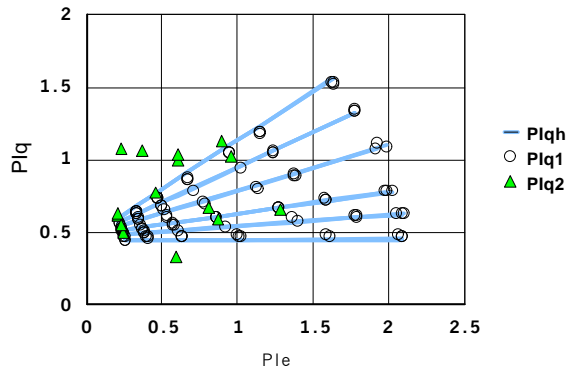


Figure 12a: Scaling plot for $b = 0.203$ m data, with fitted data, PI_{qh} (lines), measured supported jet data, PI_{q1} (circles) and PI_{q2} (triangles), where PI_{q2} has $rel > 0.1$, versus dimensionless head PI_e .

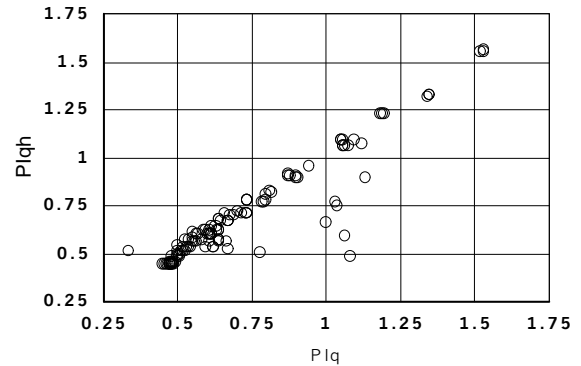


Figure 12b: Scaling plot for $b = 0.203$ m data, with fitted data, PI_{qh} versus measure supported jet data, PI_q .

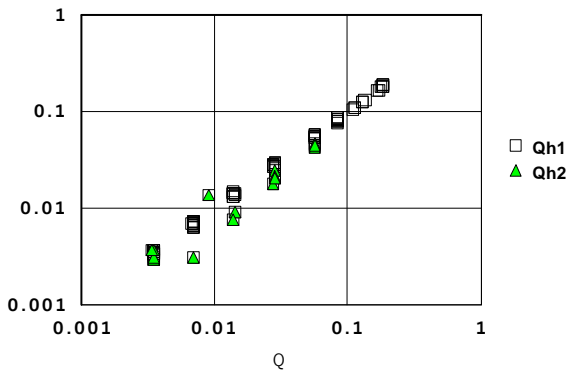


Figure 12c: Scaling plot for $b = 0.203$ m data, with fitted supported jet estimates, Q_{h1} , versus measured flows, Q (m^3/s), where Q_{h2} has $rel > 0.1$.

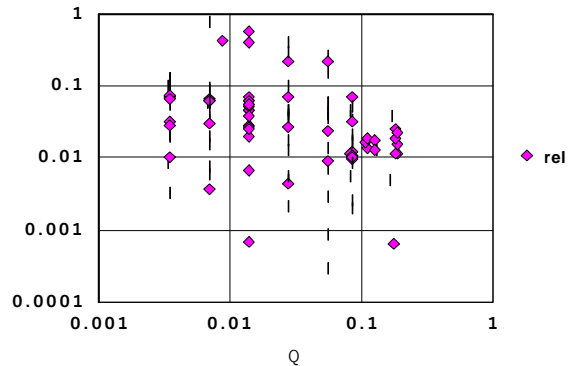


Figure 12d: Scaling plot data for $b = 0.203$ m, with relative error, rel , versus measured flow Q (m^3/s).

Figures 13a to 13c show similar data for $b = 0.813$ m (32 in). The mean relative error is $\text{rel} = 0.0360$ with a standard deviation of 0.0375. Notice that πe for this scale is smaller than for the other scales, indicating lower relative dimensionless heads and flows. For some reason for which the author has no explanation, the assumptions or the data fail and the measured flow is somewhat lower than predicted. It might be rash to make any general conclusions from this, since the data covers only a few geometries and there are only six head-discharge points per geometry.

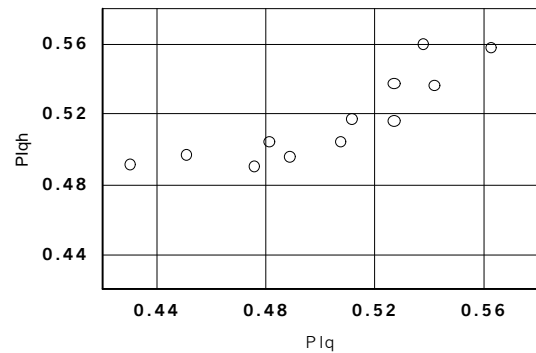
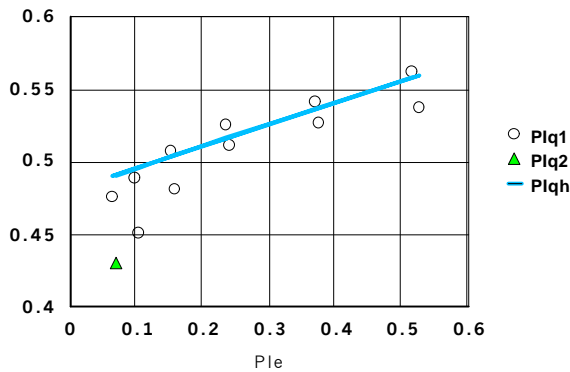


Figure 13a: Scaling plot for $b = 0.813$ m data, with fitted data, PI_{qh} (lines), and measured supported jet data, PI_{q1} and PI_{q2} versus dimensionless head, PI_e , where PI_{q2} data has $\text{rel} > 0.1$.

Figure 13b: Scaling plot with PI_{qh} versus PI_q .

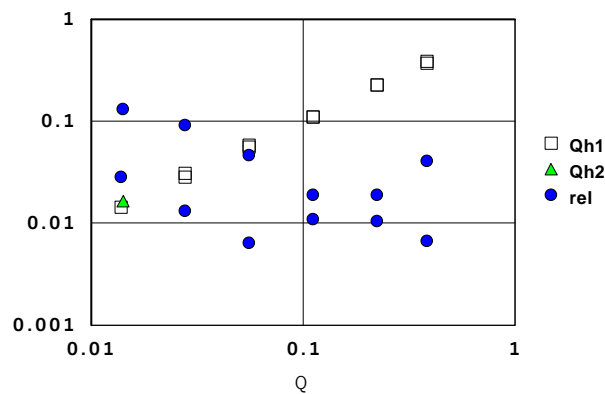


Figure 13c: Scaling plot data with fitted data, Q_{h1} and Q_{h2} , and relative error, rel , versus measured supported jet data, Q (m^3/s), where $\text{rel} > 0.1$ for Q_{h2} .

Conclusions

The head-discharge equation fit for aerated jet data ($b = 0.406$ m) has a mean relative absolute error, $\text{mean rel} = 0.0328$ with a standard deviation of 0.0361. The values of rel for aerated jet data with $b = 0.203$ m and 0.813 m are $\text{rel} = 0.0637$ and 0.0489, with standard deviations of 0.0786 and 0.0481. The data for which it is obvious that there is some partial support of the jet due to a presumed lack of aeration are excluded from these numbers, and left for later analysis, since they obey much different equations. The head-discharge equation fit for fully supported jet data ($b = 0.406$ m) has a mean relative absolute error, $\text{mean rel} = 0.0239$, with a standard deviation of 0.0282. The values of rel for fully supported jet data with $b = 0.203$ and 0.813 m are $\text{rel} = 0.0659$ and 0.0360 with standard deviations of 0.1152 and 0.0375. This is somewhat larger than the estimated flow measurement error of 1.3%, but not unusable. Whether or not this level of error is acceptable is for users or future experiments to determine. But it seems that simulated annealing is very useful in this way to determine the primary effects of such an experiment.

Acknowledgements

This work is a revision of analysis done while the author was a postdoctoral associate at the USDA-ARS Hydraulic Engineering Research Unit in Stillwater, OK. The author did not take any of the physical measurements and appreciates the efforts of Mr. Bob Sappington and Mr. Kevin Cook of the HERU in bringing him up to speed on the data. The author thanks the Agricultural Research Service for the opportunity to expand his horizons. Neither the USDA Agricultural Research Service, nor any of its employees, nor any of their awardees, subcontractors, or their employees, makes any warranty, express or implied, or assumes any

legal liability or responsibility for the accuracy, completeness, or usefulness of any information, apparatus, product or process disclosed here, or represents that its use would not infringe on privately-owned rights.

References

- Ackers, P., W.R. White, J.A. Perkins and A.J.M. Harrison (1978). *Weir and Flumes for Flow Measurement*. John Wiley and Sons, New York. ISBN 0-471-99637-8.
- Fread, D.L. (1991). "BREACH, An erosion model for earthen dam failures. (Revision 1, August 1991)" <http://www.nws.noaa.gov/oh/hrl/rvrmech/documentation/breach.pdf>
- Goffe, W.L., G.D. Ferrier and J. Rogers (1994). "Global optimization of statistical functions with simulated annealing". *Journal of Econometrics*, 60(1/2):65-99.
- Gupta, R.S. (1989) *Hydrology and Hydraulic Systems*. Waveland Press, Prospect Heights, IL.
- Henderson, F.M. (1966). *Open Channel Flow*. MacMillan Publishing, New York.
- John, J.A.E. and W.L. Haberman (1988). *Introduction to Fluid Mechanics*, Prentice Hall, Engelwood Cliffs, NJ.
- Logan, J.D. (1987). *Applied Mathematics: A Contemporary Approach*. J. Wiley & Sons. New York.
- Press, W.H., B.P. Flannery, S.A. Teukolsky and W.T. Vetterling (1989). *Numerical Recipes; The Art of Scientific Computing (FORTRAN Version)*. Cambridge University Press, Cambridge.